Physica E 44 (2012) 1495–1502

Contents lists available at SciVerse ScienceDirect

Physica E

journal homepage: www.elsevier.com/locate/physe

The effect of disorder on integer quantized Hall effect

S. Erden Gulebaglan [a,*], G. Oylumluoglu [b], U. Erkaslan [b], A. Siddiki [c], I. Sökmen [a]

[a] Dokuz Eylül University, Physics Department, Faculty of Arts and Sciences, 35160 Izmir, Turkey
[b] Muğla University, Physics Department, Faculty of Arts and Sciences, 48170 Kötekli, Muğla, Turkey
[c] Istanbul University, Physics Department, Faculty of Sciences, 34134-Vezneciler-Istanbul, Turkey

ARTICLE INFO

Article history:
Received 23 September 2011
Received in revised form
13 March 2012
Accepted 13 March 2012
Available online 28 March 2012

ABSTRACT

We study the effects of disorder on the integer quantized Hall effect within the screening theory, systematically. The disorder potential is analyzed considering the range of the potential fluctuations. The short-range potential fluctuations ($\lesssim 20$ nm) stems from single impurities and defines the Landau level broadening, whereas, the long-range potential fluctuations ($\gtrsim 200$ nm) are calculated from the potential overlap of many-impurities, which in turn determines the widths of the plateaus. The short-range part is taken into account via self-consistent Born approximation hence determining the conductivities and a local version of Ohm's law is utilized to define charge transport. We investigate the long range potential fluctuations taking into account interaction effects and explore its effect on the formation of quantum Hall plateaus depending on the number of impurities, the amplitude of the impurity potential and the separation thickness by solving the 3D Poisson equation iteratively. We discuss the long range part of the potential fluctuations by investigating the Coulomb interaction of the two dimension electron gas numerically. We show that the widths of the quantized Hall plateaus increase with increasing disorder, whereas the influence of level broadening is suppressed at narrow Hall bars.

1. Introduction

The integer quantized Hall effect (IQHE), observed at two dimensional charge systems (2DCS) subject to strong perpendicular magnetic fields B, is usually discussed within the single particle picture, which relies on the fact that the system is highly disordered [1,2]. These quantized (spinless) single particle energy levels are called the Landau levels (LLs) and the discrete energy values are given by $E_N = \hbar\omega_c(n+1/2)$, where n is the Landau index and $\omega_c = eB/m^*c$ is the cyclotron frequency of an electron with an effective mass m^* ($\approx 0.067m_e$, m_e being the bare electron mass at rest) and c is the speed of light in vacuum. In single particle models the disorder plays several roles, such as Landau level broadening [3], leading to a finite longitudinal conductivity [4,5], spatial localization [6], *etc.* Disorder can be created by inhomogeneous distribution of dopant ions which essentially generates the confinement potential [7] for the electrons. In the absence of disorder, the density of states are Dirac delta-functions $D(E) = (1/2\pi l^2)\sum_{\infty}^{N=0}\delta(E-E_N)$, where $l = \sqrt{\hbar/eB}$ is the magnetic length, and the longitudinal conductivity (σ_l) vanishes. For a homogeneous two dimensional electron system (2DES), by the inclusion of disorder and due to collisions, LLs become broadened. Therefore the longitudinal conductance becomes non-zero in a finite energy (in fact magnetic field) interval. Long range potential fluctuations generated by the disorder result in the so-called *classical localization* [8], *i.e.* the guiding center of the cyclotron orbit moves along closed equi-potentials [9]. In contrast to the above mentioned bulk theories, the edge theories usually disregard the effect of disorder to explain the (quantized) Hall resistance R_H and accompanying (zero) longitudinal resistance R_L. However, the non-interacting edge theories still require disorder to provide a reasonable description of the transition between the plateaus. The Landauer–Büttiker approach (known as the edge channel picture) [10] and its direct Coulomb interaction generalized version, *i.e.* the non-self-consistent Chklovskii picture [11], also needs localization assumptions in order to obtain quantized Hall (QH) plateaus of finite width.

In this paper, we distinguish between the effects of single-impurity induced short-range potential fluctuations (SRPFs) and the many-impurity defined long-range potential fluctuations (LRPFs) on the quantized Hall plateaus. We argue that, the SRPF defines the Landau level broadening (hence the widths of incompressible strips) and conductivity tensor elements. The LRPF, which results from the overlap of the long-range part of the single-impurity potentials (*i.e.* many-impurity), determines the widths of the quantized Hall plateaus. The report is organized as

* Corresponding author. Tel.: +90 2324128666; fax: +90 2324534188.
E-mail address: sinemerden@gmail.com (S. Erden Gulebaglan).

1386-9477/$ - see front matter © 2012 Elsevier B.V. All rights reserved.
http://dx.doi.org/10.1016/j.physe.2012.03.017

follows, first we introduce the single-impurity potential by comparing a Coulomb impurity with an Gaussian impurity. Next, the formalism to calculate the level broadening and conductivities, namely the self-consistent Born approximation, is revisited, together with a brief introduction to local Ohm's law and its connection to Kubo formalism. Prior to the conclusion, we present our numerical calculations, where the widths of the quantized Hall plateaus are investigated in light of our findings.

2. Model

2.1. Single-impurity

The disorder potential experienced by the 2DES resulting from the impurities has quite complicated range dependencies. Since, the potential generated by an impurity is *damped* by the dielectric material in between the impurity and the plane where the 2DES resides is screened by the homogeneous 2DES depending on the density of states, which changes drastically with and without magnetic field. Moreover, depending on the single impurity potential the landscape of the total disorder potential profile varies considerably. It is common to theoreticians to calculate the conductivities from single impurity potentials, such as Gaussian [12], Lorentzian [13] or any other analytical functions [14]. However, as it will be discussed, the landscape of potential fluctuations is also important to define the actual mobility of the sample.

Here we point to the effect of the spacer thickness on the impurity potential experienced in the plane of 2DES. It is well known from experimental and theoretical investigations that, if the distance between the electrons and donors is large, the mobility is relatively high and it is usually related with suppression of the short range fluctuations of the disorder potential. These results agree with the experimental observations of high mobility samples and are easy to understand from the z dependence of the Fourier expansion of the Coulomb potential

$$V^{\vec{q}}(z) = \int d\vec{r}\; e^{-i\vec{q}\cdot\vec{r}} \sum_{j}^{N} \frac{e^2/\overline{\kappa}}{\sqrt{(\vec{r}-\vec{r}_j)^2+z^2}} = \frac{2\pi e^2}{\overline{\kappa} q} e^{-|qz|} NS(\vec{q}), \tag{1}$$

where $S(\vec{q})$ (structural function) contains all the information about the in-plane donor distribution and N is the total number of the ionized donors. We observe that if the spacer thickness is increased, the amplitude of the potential decreases rapidly. We also see that the short range potential fluctuations, which correspond to higher order Fourier components, are suppressed more efficiently.

Consider a case where the q component approaches to zero, then the external (damped) potential is well screened, hence the long range part of the disorder potential. Whereas, the short range part remains unaffected, *i.e.* high q Fourier components. Now we turn our attention to the second type of impurities considered, the Gaussian ones. As well known, the Fourier transform of a Gaussian is also of the form of a Gaussian, therefore, similar arguments also hold for this kind of impurity.

We should emphasize once more the clear distinction between the effect of the spacer on the external potential and the screening by the 2DES, *i.e.* via $\epsilon(q)$ (the dielectric constant). The former depends on the Fourier transform of the Coulomb potential and the important effect is the different decays of the different Fourier components (see Eq. (1)), so that the short range part of the disorder potential is well dampened, whereas the latter depends on the relevant DOS of the 2DES and the screening is more effective for the long range part.

In the following, we will first compare the range dependency of a single-impurity by considering a Coulomb and a Gaussian type potentials. We will show that, if one utilizes the Gaussian potential to define the level broadening, the contribution to transport properties from the long-range part of the single-impurity potential is underestimated. Hence, should be taken into account while calculating the global resistances.

2.2. Coulomb vs. Gaussian

The electrostatic potential at (x_0,y_0,z_0), created by a single, positively charged particle (ionized donor) placed at x,y,z_D is given by

$$V(x_0,y_0,z_0) = \frac{e^2/\overline{\kappa}}{\sqrt{(x_0-x)^2+(y_0-y)^2+(z_0-z_D)^2}}, \tag{2}$$

where z_D and z_0 labels the z position of the donor layer and the electron gas, respectively, and $\overline{\kappa}$ is the average dielectric constant (~ 12.4 for GaAs). Throughout this paper we assume that the 2DES resides on $z=z_0=0$ plane and the donors are placed at a finite distance (spacer thickness) $z_D>0$, hence, the divergencies that may occur at the above equation are ruled out. In principle Eq. (2) provides a correct description of the impurity potential generated by an ionized donor, however, unfortunately such a description is not useful to define conductivities analytically [12]. Instead, one usually considers a Gaussian impurity with an potential amplitude $V_{\rm imp}$ generating a potential at the (x_0,y_0) plane

$$V(x_0,y_0,0) = -\frac{e^2 V_{\rm imp}}{\overline{\kappa}|z_D|} \exp\left[-\frac{(x_0-x)^2+(y_0-y)^2}{2z_D^2}\right]. \tag{3}$$

These potentials are shown in Fig. 1 for a unit cell of a square lattice with a relevant average dielectric constant $\overline{\kappa}$ considering a

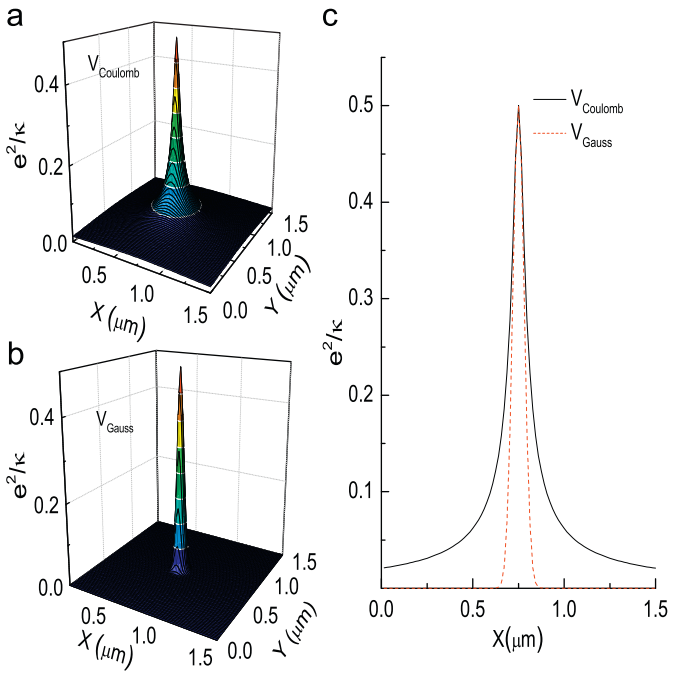

Fig. 1. A single Coulomb (a) and a Gaussian impurity (b) located at the center of a 1.5 μm × 1.5 μm unit cell, approximately 30 nm above the electron gas ($z=z_0=0$). The short range behaviors are similar, whereas long range parts are strongly different. Potential profiles projected through the center (x, $y=0.75$ μm), for the Coulomb (solid (black) line) and Gaussian impurity (broken (red) line). (For interpretation of the references to color in this figure legend, the reader is referred to the web version of this article.)

single donor residing at the center. Since, the donor is at a finite distance from the plane where the electrostatic potential is calculated, no singularity is observed in the potential distribution. We should note that the electrostatic potential created by the donor is *damped* (we use the term damped, not to mix with screened) by the dielectric material, which resides between the donor layer and the plane where we calculate the potential. The Coulomb potential presents long range part, which leads to long range fluctuations due to overlapping if several donors are considered within the unit cell, whereas, the Gaussian potential decays exponentially on the length scale comparable with the separation thickness.

The comparison of these two potential enables us to quantitatively distinguish between the short and long range parts of the single-impurity potential. In addition, from this comparison we can easily estimate the strength of the single impurity potential V_{imp}. For instance, given the experimental parameter where the donor layer resides (z_D=30 nm), one can calculate the amplitude of a single-impurity potential to be 0.033 eV, which we will use when calculating the conductivities and long-range potential fluctuations.

2.3. Level broadening and conductivities

The electron-impurity scattering at high magnetic fields and low temperatures is a long discussed phenomena as mentioned in the Introduction. However, in the case of non-overlapping Landau levels and short-range impurities self-consistent Born approximation provides a reasonable framework to calculate the effect of disorder on level broadening and on conductivities, which can be summarized in the following. Assuming a Gaussian single-impurity and calculating Green's function of the Landau hamiltonian one can obtain the spectral function as [4]

$$A_n(E)=\frac{2}{\pi\Gamma_n}\sqrt{1-\left(\frac{E-E_n}{\Gamma_n}\right)^2}, \tag{4}$$

where Γ_n is the width of the Landau level and is obtained from the Laguerre polynomials as

$$\Gamma_n^2=(\Gamma_n^{(0)})^2=\Gamma^2\int_0^\infty dx\,[L_n^0((R_{rmg}/l)^2x)]^2\,\exp(-[1+(R_g/l)^2]x), \tag{5}$$

and R_g is the range of the single-impurity with a Gaussian profile. Starting from the spectral function one can calculate the longitudinal conductivity

$$\sigma_l=2\sum_{n=0}^{\infty}\int dE\left[-\frac{\partial f}{\partial E}\right]\sigma_{xx}^{(n)}(E), \tag{6}$$

and the Hall conductivity

$$\sigma_H=\frac{e^2}{h}2\pi l^2 n_{\rm el}-\Delta\sigma_H. \tag{7}$$

here $\sigma_{xx}^{(n)}(E)$ is the contribution from each Landau level as a function of energy and $\Delta\sigma_H$ is the quantum mechanical correction to the classical Hall conductivity. The explicit forms of the conductivities can be found in the existing literature [4,5,12,17]. We will utilize the above conductivities to calculate global resistances in the following.

Equipped with the information about the short-range potential influencing the level broadening conductivities, next we investigate the overall impact of disorder potential on the electronic system. First, we will numerically investigate the potential landscape generated by many Coulombic impurities and then by subtracting the Gaussian-like short-range part, we will explore the effect of remaining long-range part on plateau widths.

2.4. Many-impurity and interactions

We continue our investigation by solving the 3D Poisson equation iteratively for randomly distributed single impurities, where three descriptive parameters (*i.e.* the number of impurities, the amplitude of the impurity potential and the separation thickness) are analyzed separately. The total potential is given by

$$V(x,y,z)=V_D(x,y,z)+V_D(x,y,z), \tag{8}$$

here we assume that the locations of the single impurities are fixed and the donor potential is given by

$$V_D(x,y,z)=\sum_{i=1}^{N_{\rm imp}}V_{\rm imp}^{(i)}(x_i,y_i,z_i), \tag{9}$$

we furthermore assume that all the single-impurities reside at the same layer, *i.e.* $z_i=z_D$. For the electronic potential one has to calculate the Hartree potential given by

$$V_D(x,y,z)=\int_{\rm Vol}dx'\,dy'\,dz'\,n_{\rm el}(x',y',z')K(x,y,z;x',y',z'), \tag{10}$$

where $K(x,y,z;x',y',z')$ is the solution of the Poisson equation for the given boundary conditions and is calculated numerically described below.

To obtain the potential landscape generated by many-impurities also taking into account interaction effects, we solve the Poisson equation in 3D starting from the material properties of the wafer under investigation. The typical material we consider is sketched in Fig. 2. In our calculation scheme, we use the growth parameters and construct a 3D lattice where the potential and the charge distributions are obtained iteratively assuming open boundary conditions, *i.e.* $V(x\to\pm\infty,y\to\pm\infty,z\to\pm\infty)=0$. For such boundary conditions, we chose a lattice size which is considerably larger than the region that we are interested in. We preserve the above conditions within a good numerical accuracy (absolute error of 10^{-6}). A forth order grid approach [15] is used to reduce the computational time, which is successfully used to describe similar structures [16]. The calculation scheme can be briefly summarized as follows: we first generate a 3D matrix, where the heterostructure is embedded in a dielectric material (for this case air) so that the above boundary conditions are satisfied. In the next step the donors are located randomly on the grid together with the electron layer assuming a

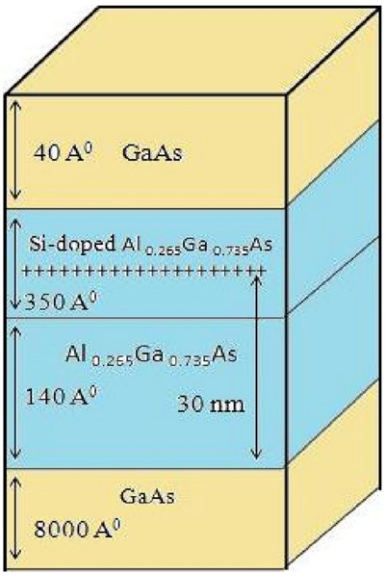

Fig. 2. Sketch of the crystal, which we investigate numerically. The crystal is spanned by a 3D matrix (128 × 128 × 60).

homogeneous distribution, the Poisson equation is solved for the given boundary conditions. The resulting potential is used to calculate the new distribution of electrons, hence the new potential distribution. Once the potential and charge distributions are not changed (within the numerical accuracy) at the last iteration step. Fig. 2 presents the schematic drawing of the heterostructure which we are interested in. The donor layer is δ-doped by a density of 3.3×10^{16} m^{-2} (ionized) Silicon atoms, $\sim$30 nm above the 2DES, which provide electrons both for the potential well at the interface and the surface. It is worthwhile to note that most of the electrons ($\sim$90%) escape to the surface to pin the Fermi energy to the mid-gap of the GaAs. In any case, for such wafer parameters there are sufficient number of electrons ($n_{el}\gtrsim 3.0\times10^{15}$ m^{-2}) at the quantum well to form a 2DES. To investigate the effect of impurities we place positively charged ions at the layer where donors reside. From Eq. (1) we estimate the amplitude of the potential of a single impurity to be $(e^2/\kappa)(V_{imp}/z_D)=0.033$ eV and assume that *some* percent of the ionized donors are generating the disorder potential, that defines the long range fluctuations. In our simulations we perform calculations for a unit cell with lateral size of 1.5 μm × 1.5 μm which contains 3.3×10^{16} donors/m^2, thus with a 10% disorder we should have N_I 3300 impurities. The calculations are repeated considering many randomly distributed (up to 200 times, depending on the number of impurities) impurity configurations and the long-range parts are extracted from the average distances between the extremum obtained from these different configurations. In addition, to test the viability of the statistical averaging different sets of randomly distributed configurations are also tested.

Fig. 3a depicts the actual density distribution, when considering 3300 impurities, whereas Fig. 3b presents only the long range part of the density fluctuation. The arrows show the average distance between two maxima, which is calculated approximately to be 550 nm. To estimate an average range of the disorder potential, we repeated calculations for such randomly distributed impurities, where number of repetitions scales with $\sqrt{N_I}$. Such a statistical investigation sufficiently ensembles the system to provide a reasonable estimation of the long range fluctuations. We also tested for larger number of random distributions, however, the estimation deviated less than tens of nanometers. We show our main result of this section in Fig. 4, where we plot the estimated long range part of the disorder potential considering various number of impurities N_I and impurity potential amplitude

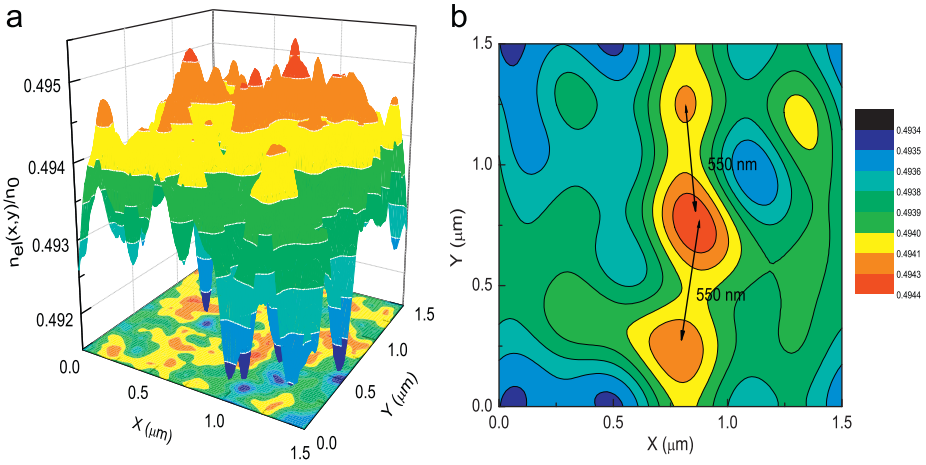

Fig. 3. (a) Electron density fluctuation considering 3300 impurities at the sketch of the crystal. (b) The long-range part, arrows are to guide the distance between two maxima. The calculation is repeated for 50 random distributions, which lead to a similar long range.

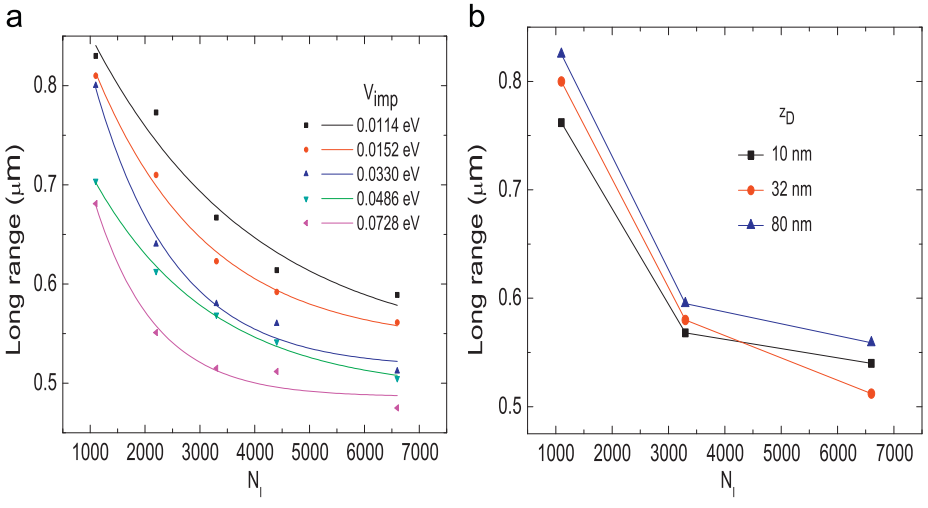

Fig. 4. Statistically estimated range of the density fluctuations as a function of number of impurities, considering various impurity strengths (a) and spacer thicknesses (b). The calculations are done at zero temperature considering Coulomb impurities. The long range potential fluctuations become larger than the size of the unit cell if one considers less than 5% disorder.

V_{imp}. Our first observation is that the long range part of the total potential becomes less when N_I becomes large, not surprisingly. However, the range increases nonlinearly while decreasing N_I, obeying almost an inverse square law and tends to saturate at highly disordered system. When fixing the distributions and N_I, and changing the amplitude of the impurity potential we observe that for large amplitudes the range can differ as large as 200 nm at all impurity densities. We found that for an impurity concentration less than 3%, the range of the potential is larger than the unit cell we consider, *i.e.* $R > 1.5$ μm. In contrast to the long range part, the short range part is almost unaffected by the impurity concentration, however, is affected by the amplitude. Therefore, while defining the conductivities we will focus our investigation on V_{imp}. Another important result is that the estimates of long range fluctuations do not depend strongly on the spacer thickness, if one keeps the amplitude of single impurity potential amplitude fixed, Fig. 4b. All of the above numerical observations coincide fairly good with our analytical investigations. We should also note that, similar or even complicated numerical calculations are present in the literature [6,7].

To summarize: we performed 3D numerical calculations to estimate the effect of impurities on the potential landscape experienced by the 2DES. We found that the range of the fluctuations strongly depend on the number of impurities. If one adds more than 20% of impurity, the range of the potential fluctuations are less than 400–500 nm, however, this (short) range is affected by the amplitude of single impurity potential. Whereas, if only few percent of disorder is considered the range becomes approximately more than 650 nm. In contrast to the highly disordered case, the amplitude of single impurity potential is less pronounced. The spacer thickness seems not to play an important role in defining the range of the potential fluctuations, while keeping V_{imp} constant. In addition, performing 3D calculations also enables us to estimate the strength of the long-range potential fluctuations. We observed that, once the number of impurities increase, the variation of the potential also increases. We calculated this variation by finding the difference between a purely clean sample and the depth of the maximum (or minimum) once impurities are taken into account. This is what one would expect also from Eq. (2), our numerical results show that the amplitude of the potential variations change between few percents of the Fermi energy to at most 50%. We will use these values to simulate the long-range potential fluctuations considering different mobilities.

Next section is devoted to investigate the widths of the quantized Hall plateaus utilizing our findings. We consider mainly two "mobility" regimes, where the long range fluctuations is at the order of microns (high mobility) and is at the order of few hundred nanometers, low mobility. However, the amplitude of the total potential fluctuations will be estimated not only depending on the number of impurities but also depending on the spacer thickness, range and amplitude of single impurity potential.

3. Quantized Hall plateaus

The main aim of this section is to provide a systematic investigation of the quantized Hall plateau (QHP) widths within the screening theory of the IQHE [17], therefore here we summarize the essential findings of the mentioned theory. In calculating the QHPs one needs to know local conductivities, namely the longitudinal $\sigma_l(x,y)$ and the transverse $\sigma_H(x,y)$. To determine these quantities it is required to relate the electron density distribution $n_{el}(x,y)$ to the local conductivities explicitly. Here we utilize the SCBA [12]. However, the calculation of the electron density and the potential distribution including direct Coulomb interaction is not straightforward, one has to solve the Schrödinger and the Poisson equations simultaneously. This is done within the Thomas–Fermi approximation which provides the following prescription to calculate the electron density:

$$n_{el}(x,y) = \int dE\, D(E) \frac{1}{e^{(E_F - V(x,y))/k_B T} + 1}, \tag{11}$$

where $D(E)$ is the appropriate density of states calculated within the SCBA, where k_B is the Boltzmann constant and T is the temperature. The total potential is obtained from

$$V(x,y) = \frac{2e^2}{\overline{\kappa}} \int dx\, dy\, K(x,y,x',y') n_{el}(x,y), \tag{12}$$

and the Kernel $K(x,y,x',y')$ is the solution of the Poisson equation satisfying the boundary conditions to be discussed next.

In the following we assume a translation in variance in y-direction and implement the boundary conditions $V(-d) = V(d) = 0$ ($2d$ being the sample width), proposed by Chklovskii et al. [11], such a geometry allows us to calculate the Kernel in a closed form. Hence, Eqs. (11) and (12) form the self-consistency. For a given initial potential distribution, the electron concentration can be calculated at finite temperature and magnetic field, where the density of states $D(E)$ contains the information about the quantizing magnetic field and the effect of short range impurities. Here we implicitly assume that the electrons reside in the interval $-b < x < b$, and is fixed by the Fermi energy, *i.e.* the number of electrons, hence donors. As a direct consequence of Landau quantization and the locally varying electrostatic potential, the electronic system is separated into two distinct regions, when solving the above self-consistent equations iteratively: (i) the Fermi energy equals to (spin degenerate) Landau energy and due to DOS the system illustrates a metallic behavior, the compressible region, (ii) the insulator like incompressible region, where E_F falls in between two consequent eigenenergies and no states are available [11,18]. It is usual to define the filling factor ν, to express the electron density in terms of the applied B field as, $\nu = 2\pi l^2 n_{el}$. Since all the states below the Fermi energy are occupied the filling factor of the incompressible regions correspond to integer values (*e.g.* $\nu = 2, 4, 6, \ldots$), whereas the compressible regions have non-integer values, due to partially occupied higher most Landau level. The spatial distribution and widths of these regions are determined by the confinement potential [11], magnetic field [19], temperature [20] and level broadening [13,17]. For the purpose of the present work we fix the confinement potential profile by confining ourselves to the Chklovskii geometry and keeping the donor concentration (and distribution) constant. Moreover we perform our calculations at a default temperature given by $k_B T/E_F^0 = 0.02$, where E_F^0 is the Fermi energy calculated for the electron concentration at the center of the sample and is typically similar to 10 meV. In addition, the Fermi energy is $E_F^0 = n_{el}(0; B = 0, T = 0)/D_0$ corresponding to the electron density at the center and $D_0 = m/(\pi\hbar^2)$ the DOS of the 2DES at $B = 0$.

3.1. Transport within the local Ohm's law

The next step is to calculate the global resistances, *i.e.* the longitudinal R_L and Hall R_H resistances, starting from the local conductivity tensor elements. Such a calculation is done within a relaxed local model that relates the current densities $\mathbf{j}(x,y)$ to the electric fields $\mathbf{E}(x,y)$, namely the local Ohm's law

$$\mathbf{j}(x,y) = \hat{\sigma}(x,y)\mathbf{E}(x,y). \tag{13}$$

The strict locality of the conductivity model is lifted by an spatial averaging process [17] over the quantum mechanical length

scales and an averaged conductivity tensor $\hat{\tilde{\sigma}}(x,y)$ is used to obtain the global resistances. It should be emphasized that, such an averaging process also simulates the quantum mechanical effects on the electrostatic quantities. To be explicit: if the widths of the current carrying incompressible strips become narrower than the extend of the wave functions, these strips become "leaky" which cannot decouple the two sides of the Hall bar and back-scattering takes place. Therefore, to simulate the "leakiness" of the incompressible strips we perform coarse-graining over quantum mechanical length scales. Now let us relate the local conductivities with the local filling factors. Since the compressible regions behave like a metal within these regions there is finite scattering leading to finite conductivity. In contrast, within the incompressible regions the back-scattering is absent, hence, the longitudinal conductivity (and simultaneously resistivity) vanishes. Therefore, all the imposed current is confined to these regions. The Hall conductivity meanwhile is just proportional to the local electron density. The explicit forms of the conductivity tensor elements are presented elsewhere [17]. Having the electron density and local magneto-transport coefficients at hand, we perform calculations to obtain the widths of the quantized Hall plateaus utilizing the above described, microscopic model assisted by the local Ohm's law at a fixed external current I.

It is worth to comment on the connection between the above described local Ohm's law approach with the well known Kubo formalism. The local Ohm's law is a semi-classical approach to describe electron transport at quantizing high magnetic fields, in the sense that the electronic levels are quantized, however, the center of mass (or the center coordinate) motion is treated classically. This is justified once time scales related with the drift velocity is much smaller than the time scales related with the cyclotron motion. In other words, the local Ohm's law is just the well known Born–Oppenheimer approximation and is a limit of the Kubo formalism for transport apart from the fact the later is limited for the linear response regime, however, when applicable local Ohm's law geos beyond this limit under above mentioned conditions.

3.2. Single impurity potentials: level broadening and conductivities

Since the very early days of the charge transport theory, collisions played an important role. Such a scattering based definition of conduction also applies for the system at hand, *i.e.* a two-dimensional electron gas subject to perpendicular magnetic field. Among many other approaches [13,21] the SCBA emerged as a reasonable model to describe the DOS assuming Gaussian impurities, considering short range scattering, as discussed previously. A single impurity has two distinct parameters that represents the properties of the resulting potential, the range R_g (at the order of separation thickness) and impurity potential amplitude (in relevant units), $\tilde{V}_{\mathrm{imp}}$. However, these two parameters are not enough to define the widths of the Landau levels (Γ), another important parameter is the number of the impurities, N_I. In the previous section we have already investigated these three parameters in scope of potential landscape, now we utilize our findings to define the level widths and the conductivities. It is more convenient to write the single impurity potential of the form

$$V_g(r) = \frac{\tilde{V}_{\mathrm{imp}}}{\pi R_g^2} \exp\left(-\frac{r^2}{R_g^2}\right). \tag{14}$$

Together with the impurity concentration, the relaxation time is defined as $\tau_0 = \hbar^3/N_I\tilde{V}_{\mathrm{imp}}^2 m^*$ and in the limit of delta impurities (*i.e.* $R_g \to 0$) the Landau level width Γ takes the form $\Gamma = \sqrt{4N_I\tilde{V}_{\mathrm{imp}}^2/2\pi l^2}$. It is useful to define the impurity strength parameter to investigate the effect of disorder by

$$\gamma_I^2 = (\Gamma/\hbar\omega_c)^2 = \frac{2N_I\tilde{V}_{\mathrm{imp}}^2 m}{\pi\hbar^3\omega_c}, \tag{15}$$

given in units of cyclotron energy $\hbar\omega_c = \hbar eB/m = \Omega_c$ and as a normalization parameter we fix the cyclotron energy at 10 Tesla. The details of the calculation scheme are described in detail elsewhere [17].

3.3. Many impurities: potential fluctuations

We have investigated the effect of single impurity potentials on the overall potential landscape. We have seen that, at high impurity concentration the overall potential fluctuates over a length scale of couple of hundred nanometers, whereas for low N_I concentration such length scale can be as large as micrometers. Now we include the effect of this long range potential fluctuations *into* our screening calculations via modulation potential defined as $V_{\mathrm{mod}}(x) = V_0 \cos(2\pi x m_p/2d)$, where the inverse modulation period m_p is chosen such that the boundary conditions are preserved. At the moment, we consider two modulation periods regardless of the sample width and vary the amplitude of the modulation potential.

Our investigation of the impurities leads us to conclude that one has to define mobility at high magnetic fields also taking into account screening effects in general and furthermore also the geometric properties of the sample such as the width and depletion length. The distinguishing parts can be summarized as follows, in single-impurity approaches the mobility is only defined by the scattering time (*i.e.* the momentum relaxation time), which is calculated from the bare disorder potential. On the other hand, once interactions and screening effects are taken into account one should also consider the effects stemming from the overlap of long-range part of the many-impurity potentials. We have calculated the properties of these two parts of the disorder potential and found that, if the single-impurity potentials are assumed to have Gaussian forms one can calculate the (local) level broadening (and hence local conductivities) accurately. However, the difference between the real Coulomb impurities and the assumed Gaussian impurities become important considering the long-range part of the disorder potential. Hence, based on our numerical results we estimate that the mobility of the sample should be defined depending on these different parts of the disorder potential. Therefore, in the following we will investigate the effect of the disorder potential on the global resistances by (i) accounting the short-range part within the level broadening and (ii) the long-range part in our screening calculations.

4. Discussion

In this final section, we harvest our findings of the previous sections to make quantitative estimations of the plateau widths, considering narrow gate defined samples. Our aim is to show the qualitative and quantitative differences between "high" and "low" mobility samples, by taking into account properties of the single impurity potentials and the resulting disorder potential. The experimental realizations of these samples are reported in the literature [22,23]. We estimated that the range of the potential fluctuations is less than 500 nm for low mobility ($N_I > 3300$) and is greater than 1 μm at high mobility. Therefore, the modulation period is chosen such that many oscillations correspond to low mobility, and few oscillations correspond high mobility. As an specific example let us consider a 10 μm sample, for the low mobility we choose $m_p = 19-20$ and for the high mobility m_p is taken as 9 or 10. The amplitude of the disorder potential is

damped to 50% of the Fermi energy when considering the effect of spacer thickness, however, including screening this amplitude is further reduced to few percents. In light of this estimations the low mobility will be presented by a modulation amplitude of $V_0/E_F^0 = 0.5$, whereas high mobility corresponds to $V_0/E_F^0 = 0.05$. Therefore, we have four different combinations of the disorder potential parameters yielding four different mobilities considering two sample widths, as tabulated in Table 1. The second important aspect of the disorder is the single impurity parameters, for low mobility set we choose $R_g = 20$ nm and $\gamma_I = 0.3$, whereas for high mobility $R_g = 10$ nm and $\gamma_I = 0.05$ is set. Fig. 5 summarizes our results considering above discussed mobility regimes for two different sample widths. In Fig. 5a, we show the calculated Hall resistances for a sample of 10 μm with the highest mobility (solid (black) line) and intermediate 1 mobility (broken (red) line). The solid line is the highest mobility since the range of the fluctuations are at the order of 1 μm and the amplitude of the modulation potential is 5% of the Fermi energy. The broken line presents the intermediate mobility considering a modulation amplitude of $0.5E_F^0$. We observe that the lower mobility wafer presents a larger quantized Hall plateau, which is now in complete agreement with the experimental results [22,23]. Moreover, our calculation scheme is free of localization assumptions in contrast to the known literature and we only considered a very limited level broadening, *i.e.* $\gamma_I = 0.05$. In fact our results also hold for Dirac-delta Landau levels, however, for the sake of consistency we choose the broadening parameters according to the selected disorder parameters. In Fig. 5c, we show two curves for even lower mobilities, the solid line corresponds to the intermediate 2 case, whereas the broken line is the lowest mobility considered here. The potential fluctuation range (*i.e.* the modulation period) is chosen to present the low mobility wafer. We again see that for the lowest mobility the quantized Hall plateau is enlarged considerably from both edges of the plateau. These results explicitly show that the quantized Hall plateaus become broader if one strongly modulates the electronic system by long range potential fluctuations, either by changing the range *or* the amplitude of the modulation. Similar results are also obtained for a relatively narrower sample $2d = 3$ μm, Fig. 5b and d, however, we see that decreasing the range of the potential fluctuation is more efficient in enlarging the quantized Hall plateaus when compared to the effect of the amplitude of the modulation.

Table 1
A qualitative comparison of the mobility in the presence of magnetic field also taking into account self-consistent screening. Mobility also depends on the size of the sample when screening is also considered.

Mobility	m_p (d = 10 μm)	m_p (d = 2 μm)	V_0/E_F^0
Low	19–20	5–6	0.5
Intermediate 1	9–10	2–3	0.5
Intermediate 2	19–20	5–6	0.05
High	9–10	2–3	0.05

5. Conclusions

We performed 3D numerical calculations to estimate the effect of impurities on the potential landscape experienced by the 2DES. We found that the range of the fluctuations strongly depend on the number of impurities. For highly disordered case, the

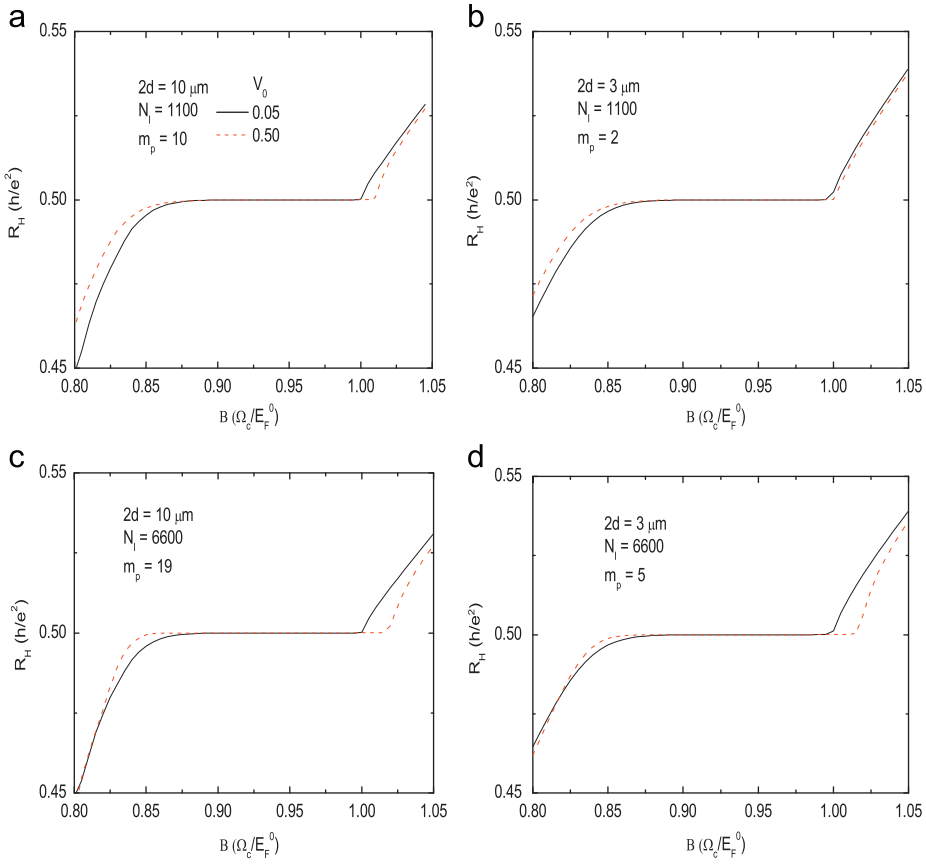

Fig. 5. Line plots of the Hall resistance as a function of magnetic field considering two sample widths ($2d = 10$ μm left panels, $2d = 3$ μm right panels) and impurity concentrations (~3% (a) and (b), ~20% (c) and (d)). Here the single impurity parameters are calculated from Eq. (15), otherwise other parameters are the same. (For interpretation of the references to color in this figure legend, the reader is referred to the web version of this article.)

amplitude of single impurity potential is less pronounced. The spacer thickness seems not to play an important role in defining the range of the potential fluctuations, while keeping V_{imp} constant.

In this work we tackled with the long standing and widely discussed question of the effect of disorder on the quantized Hall plateaus. The distinguishing aspect of our approach relies on the separate treatment of the long range fluctuations of the disorder potential. We show that assuming Gaussian impurities is not sufficient to describe long range potential fluctuations, however, is adequate to give a prescription in defining the density of states broadening and conductivities. The discrepancy in handling the long range potential fluctuations is cured by the inclusion of a modulation potential to the self-consistent calculations. We estimated the range of these fluctuations from our analytical and numerical calculations considering the effect of dielectric spacer and the screening of the 2DES and the direct Coulomb interaction is dominant in screening the long range fluctuations.

Acknowledgments

This work was partially supported by the Scientific and Technical Research Council of Turkey (TÜBİTAK) under Grant no. 109T083, IU-BAP:6970.

References

[1] B. Kramer, S. Kettemann, T. Ohtsuki, Physica E 20 (2003) 172.
[2] L. Schweitzer, B. Kramer, A. MacKinnon, Zeitschrift für Physik B 59 (1985) 379.
[3] W. Cai, C.S. Ting, Physical Review B 33 (1986) 3967.
[4] T. Ando, Y. Uemura, Journal of the Physical Society of Japan 36 (1974) 959.
[5] T. Ando, Y. Matsumoto, Y. Uemura, Journal of the Physical Society of Japan 39 (1975) 279.
[6] J.A. Nixon, J.H. Davies, Physical Review B 41 (1990) 7929.
[7] M. Stopa, Y. Aoyagi, Physica B: Condensed Matter 227 (1996) 61.
[8] M.M. Fogler, B.I. Shklovskii, Physical Review B 50 (1994) 1656.
[9] A.L. Efros, Solid State Communications 67 (1988) 1019.
[10] M. Büttiker, Physical Review Letters 57 (1986) 1761.
[11] D.B. Chklovskii, B.I. Shklovskii, L.I. Glazman, Physical Review B 46 (1992) 4026.
[12] T. Ando, A.B. Fowler, F. Stern, Reviews of Modern Physics 54 (1982) 437.
[13] K. Güven, R.R. Gerhardts, Physical Review B 67 (2003) 115327:1.
[14] T. Champel, S. Florens, L. Canet, Physical Review B 78 (2008) 125302.
[15] A. Weichselbaum, S.E. Ulloa, Physical Review E 68 (2003) 056707.
[16] S. Arslan, E. Cicek, D. Eksi, S. Aktas, Physical Review B 78 (2008) 125423:1.
[17] A. Siddiki, R.R. Gerhardts, Physical Review B 70 (2004) 195335.
[18] A. Siddiki, R.R. Gerhadts, Physical Review B 68 (2003) 125315:1.
[19] K. Lier, R.R. Gerhardts, Physical Review B 50 (1994) 7757.
[20] J.H. Oh, R.R. Gerhardts, Physical Review B 56 (1997) 13519.
[21] R.R. Gerhardts, Zeitschrift für Physik B 21 (1975) 285.
[22] J. Horas, A. Siddiki, J. Moser, W. Wegscheider, S. Ludwig, Physica E—Low Dimensional Systems and Nanostructures 40 (2008) 1130.
[23] A. Siddiki, J. Horas, J. Moser, W. Wegscheider, S. Ludwig, Europhysics Letters 88 (2009) 17007:1.